© L. Pratt and J. Whitehead 7/27/06
very rough draft-not for distribution

2.5 Constant potential vorticity flow from a wide basin: Gill's model.

The Whitehead, Leetma and Knox (WLK) model was followed three years hence by a more elaborate treatment due to Gill (1977). In addition to his model, detailed below, Gill introduced a unifying framework for treating hydraulics problems. We have made repeated use of his formalism, particularly in the derivation of conditions for hydraulic criticality. This material was reviewed and generalized in Section 1.5. The model developed by Gill was based on his particular view of the upstream basin and is rather more involved than that of WLK. Some investigators have found Gill's scaling and choice of upstream parameters unintuitive and have developed their own versions of his basic model. In consideration of the historical importance of Gill's paper, our preference in presenting the work is to first describe the model as originally formulated. The next section will discuss some insights that are gained from alternative formulations.

(a) Basics

The depth and velocity profiles predicted by zero potential vorticity models such as WLK are valid near the sill, where the local depth (scaled by D) is small compared to the reservoir depth D_∞. However, these expressions do not apply in the reservoir, where by hypothesis the depth *equals* D_∞. It is therefore difficult to verify the self consistency of the model, in particular the hypothesis that a quiescent, infinitely deep upstream state can be linked to the sill flow in a dynamically consistent way. In thinking about the character of the upstream flow, one might also wish to consider other possible states. Observations from deep straits such as the Faroe Bank Channel suggest the bulk of the overflow comes from intermediate water masses, which span the relatively wide upstream basin but may not be significantly thicker than the layer depth at the sill. Some or all of these realities led Gill (1977) to consider non-zero (but still uniform) values of $q(= D / D_\infty)$. The depth and velocity profiles across the channel are given by the more general forms (2.2.3) and (2.3.4), which show that the flow is confined to side-wall boundary layers of width $L_d=(gD_\infty)^{1/2}/f$. In the WLK model this width is much larger than the channel width $[fw^*/(gD_\infty)^{1/2} = q^{1/2}w << 1]$ due to the fact that $q<<1$. Most of the novel features of Gill's model can be linked to the boundary layers.

The model employs rectangular cross-sectional geometry and we analyze the case of non-separated flow first. The steady forms of (2.2.15) and (2.2.16) then require conservation of the volume transport Q and the average $\bar{B}$ of the Bernoulli function on the two walls. Since we no longer care about special values or limits of D (such as $D<<D_\infty$) we are free to set it to any convenient value. The choice $D= (fQ^*/2g)^{1/2}$ is convenient as it is equivalent to setting Q=2 (see Exercise 1) in the statement of conservation of mass (2.2.18). Therefore

$$\bar{d}\hat{d} = 1. \qquad (2.5.1)$$

© L. Pratt and J. Whitehead 7/27/06
very rough draft-not for distribution

In addition, conservation of the energy (2.2.16 and 2.2.17) for the steady flow implies

$$\tfrac{1}{2}q[T^{-2}\hat{d}^2 + T^2(\bar{d} - q^{-1})^2] + \bar{d} + h = \bar{B}\,, \qquad (2.5.2)$$

where again $T = \tanh(\tfrac{1}{2}q^{1/2}w)$. Eliminating $\hat{d}$ from these two equations gives

$$T^2(\bar{d} - q^{-1})^2 + \frac{1}{T^2\bar{d}^2} + 2q^{-1}(\bar{d} + h) = 2q^{-1}\bar{B}\,. \qquad (2.5.3)$$

The parameter $\bar{B}$ is generally neither a convenient nor intuitive measure of the reservoir state. If the reservoir is much wider than L_d, the flow there will be confined to side wall layers (Figure 2.5.1). The physical separation of the boundary layers makes it difficult to see how $\bar{B}$ would be specified in a laboratory experiment or oceanic setting. Furthermore, the velocity along each wall is generally non-zero (in the inviscid model) and the Bernoulli functions there may no longer be dominated by the potential energy terms $h+d$, as assumed in the WLK model. Only in the interior of the reservoir, at a distance $>> L_d$ from either wall, will the velocity be small. There, the dimensional depth is D_∞ (or $d=q^{-1}$) according to (2.2.12). With these ideas in mind, Gill (1977) suggested that a new parameter measuring the partitioning of the volume transports of each boundary layers would be more descriptive than $\bar{B}$. Some other choices are discussed in the next section.

Let the transport streamfunction ψ have the value ±1 on the side walls $x=\pm w/2$, so that the total transport is 2, as assumed. Further, let ψ_i denote the value of ψ in the quiescent interior separating the two upstream boundary currents. The transports in the right- and left-hand boundary currents (facing downstream) are therefore $1-\psi_i$ and $1+\psi_i$. Included is the possibility that $|\psi_i| > 1$ in which case one of the boundary layer transports will be greater than 2 and the other will be negative. Also note that the dimensionless value of d in the reservoir interior is q^{-1}. We can write ψ_i in terms of $\bar{B}$ by first integrating $dB/d\psi = q$, yielding $B = \bar{B} + q\psi$. Then note that B $(= \tfrac{1}{2}v^2 + d + h)$ has the value q^{-1} along $\psi=\psi_i$, as follows from the evaluation of B in the quiescent region, where $v=0$, $d=q^{-1}$, and where we will take h to be zero. Thus

$$\bar{B} = q^{-1} - q\psi_i\,, \qquad (2.5.4)$$

and substitution into (2.5.3) results in

$$\mathcal{G}(\bar{d};T,h) = T^2(\bar{d} - q^{-1})^2 + \frac{1}{T^2\bar{d}^2} + 2q^{-1}(\bar{d} + h) - 2(q^{-2} - \psi_i) = 0\,. \qquad (2.5.5)$$

The function $\mathcal{G}(\bar{d};T,h)$ relates the single flow variable $\bar{d}$ to the local geometric parameters $T(w(y))$ and $h(y)$, and is therefore of the desired form. The parameters describing the upstream flow are ψ_i and the interior reservoir depth q^{-1}. In light of the particular choice of D this last parameter can also be written as $(2gD_\infty^2 / fQ^*)^{1/2}$ leading to an alternative interpretation. For a fixed interior depth D_∞ the maximum possible geostrophic transport in the left-wall boundary layer occurs when the depth along the left wall is zero. This transport is given by $Q_{\max}=gD_\infty^2 / 2f$ and therefore $q = 2(Q^* / Q^*_{\max})^{1/2}$. In summary, it is possible to think about the reservoir parameters entirely in terms of volume transports: ψ_i measures the partitioning between boundary layers and q measures the total transport relative to the maximum possible value in the left-hand boundary layer.

(b) Critical states.

Critical states are found by taking $\partial\mathcal{G} / \partial\bar{d} = 0$, resulting in

$$(1-T_c^2)q^{-1} + T_c^2\bar{d}_c = \bar{d}_c^{-3}T_c^{-2}, \qquad (2.5.6)$$

where the subscript '*c*' denotes quantities evaluated at a critical section. According to (2.2.22), the characteristic speed c_- of a Kelvin wave propagating along the left-hand ($y=w/2$) wall is

$$c_- = q^{1/2}T^{-1}\hat{d} - \bar{d}^{1/2}[1-T^2(1-q\bar{d})]^{1/2} = 0,$$

and it is simple to show that $c_-=0$ is equivalent to (2.5.6).

Gill (1977) also defined a Froude number

$$F_d = \frac{q^{1/2}T^{-1}\hat{d}}{\bar{d}^{1/2}[1-T^2(1-q\bar{d})]^{1/2}} = \frac{\bar{v}}{\bar{d}^{1/2}[1-T^2(1-q\bar{d})]^{1/2}} \qquad (2.5.7)$$

such that F_d $(<1,=1,>1)$ indicates (subcritical, critical, and supercritical) flow corresponding to c_- (<0,=0,>0). As pointed out in Section 2.2, this Froude number should not be interpreted as the ratio of an advection to relative propagation speed. However it does measure the ability of a Kelvin wave, trapped to the left wall of the channel, to propagate upstream. If F=1 this wave is stationary; if F>1 it propagates downstream.

The geometric requirements for critical flow are obtained by setting $d\mathcal{G} / dy = 0$ in (2.5.5). If the channel width is constant, critical flow can only occur where $dh / dy = 0$ as before. When h is constant the requirement becomes

$$[T_c^4(\bar{d}_c - q^{-1})^2 - \bar{d}_c^{-2}]dw / dy = 0, \qquad (2.5.8)$$

implying that $dw/dy = 0$, as at a contraction, or that the coefficient in brackets is zero. As in the WLK model, the latter implies that $v_c(w/2, y) = d_c(-w/2, y) = 0$ meaning that the flow is in the process of separating from the left wall. However, this possibility can be rejected on the same grounds as discussed in Exercise 1 or Section 2.4.

We now turn to the case of separated flow. Here $\hat{d} = \overline{d} = 1$ in view of (2.5.1) and the only dependent variable is the width parameter $T_e = \tanh(q^{1/2} w_e / 2)$, where w_e is the separated stream width. As shown by (2.3.7) and (2.3.8), the equations relating the flow to the geometry are identical to those describing non-separated flow, but with T replaced by T_e. With this replacement and with $\overline{d} = 1$, (2.5.5) leads to an altered hydraulic function:

$$\mathcal{G}(T_e; h) = T_e^{\,2}(1 - q^{-1})^2 + \frac{1}{T_e^{\,2}} + 2q^{-1}(1 + h) - 2(q^{-2} - \psi_i) = 0 . \qquad (2.5.9)$$

The channel width $w(y)$ does not enter this relation and thus the separated current width responds only to changes in bottom elevation h. If h remains constant, changes in the position of the right wall lead to identical changes in the position of the left edge of the separated flow. This property clarifies the condition implied by the vanishing of the bracketed term in (2.5.8). Along a horizontal bottom, critical separation of the flow can occur where dw/dy is non-zero since the actual width w_e of the flow becomes stationary $dw_e/dy=0$ at that point.

The conditions for critical flow are obtained by setting $\partial \mathcal{G} / \partial T_e = 0$ with $\mathcal{G}$ defined by (2.5.9) and this leads to

$$q^{-1} = 1 + T_{ec}^{-2} \qquad (2.5.10)$$

Since T_{ec} must be $<T_c$ for the critical flow to be separated, (2.5.10) requires

$$q^{-1} \geq 1 + T_c^{-2} . \qquad (2.5.11)$$

It can also be shown that separated critical flow has $v=0$ on the right wall (see Exercise 2), a property that could have been anticipated on the basis of remarks surrounding Figure 2.4.1.

It can also be shown that the long wave speeds in this case are given by

$$c_{\pm} = q^{1/2} T_e^{-1} \pm [1 - T_e^{\,2}(1 - q)]^{1/2} = 0 ,$$

which is just the expression for attached flow (*cf* 2.2.22) but with $\hat{d} = \bar{d} = 1$ and T replaced by T_e. The corresponding Froude number is

$$F = T_{ec}^{-1}[(1 - T_{ec}^2)q^{-1} + T_{ec}^2]^{-1/2} . \qquad (2.5.12)$$

(c) Examples of solutions.

Before discussing actual solutions it is worth noting several results regarding flow separations and reversals. Following the remarks made in connection with Figure 2.2.2, we know that a continuous band of current at some upstream section cannot, at some downstream section, split into multiple bands. If fluid depth in the reservoir is nonzero across the reservoir width, then the current downstream will remain in one continuous band across each section of channel. The depth may go to zero at the left wall and the current may separate there, but it may not ground at some point interior to the fluid. In addition, the along channel velocity may reverse signs only once in the interior of the flow (see Exercise 1 of Section 2.2). Finally, it can be shown (Exercise 3 of this sections) that v must remain non-negative at a critical section.

Trying to develop a detailed understanding of Gill's model over all parametric variations and channel geometries is nearly impossible. Instead we will attempt to illustrate the features of the solutions that are interesting and exhibit behavior different from that of the WLK model. To begin with, consider the case when the channel bottom is horizontal and the flow is forced only by width contractions. Equation (2.5.5) can then be solved to obtain plots of $\bar{d}$ as a function of T for various values of the interior reservoir depth q^{-1} (Figure 2.5.2). All curves have $\psi_i = 1$ so that the reservoir is drained entirely by the left-wall boundary layer. This upstream state is sometimes motivated by consideration of a dam-break problem. Imagine a barrier that is located in the channel and that separates two resting bodies of fluid, the deeper fluid extending back into our upstream reservoir. Removal of the barrier will excite a Kelvin wave that would propagate into the reservoir along the left wall and set up the draining flow. (There are a number of complicating factors that arise in such experiments. For example a finite reservoir would allow the Kelvin wave to propagate around the perimeter and reenter the channel. However, the draining flow along the left wall would at least persist for some finite time.)

The solution space of Figure 2.5.2 has been restricted to $\bar{d} \geq 1$ (non-separated flows) since changes in the properties of separated flows can only be forced by bottom topography. The curves q^{-1}=*const.* can be used to construct particular solutions for different upstream states. To determine the appropriate value of

$$q^{-1} = 2(Q^*_{\max} / Q^*)^{1/2} = 2(gD^{*2}_{\infty} / 2fQ^*)^{1/2}$$

one would need to know the flow rate Q^* and the interior reservoir depth D_∞. The values of $\bar{d}$ for a range of channel widths are then be traced out by following by corresponding

curve. Note that all the curves extend between the right edge (T=1) of the diagram, corresponding to the reservoir ($w\rightarrow\infty$), and the lower boundary $\bar{d}=1$, corresponding to a point of separation. Since the slope of the curves near the lower boundary is negative, w increases as the separation point is approached. If further increases in width occur downstream of that point the stream will separate and continue at the same width with no further changes in properties. Each solution has a supercritical branch and a subcritical branch that merge at a point determined by the critical condition (2.5.6), indicated by the dashed line. Note that this line lies above $\bar{d}=1$, indicating that all separated flows are supercritical for ψ_i=1.

Once a particular q^{-1} is selected, it is natural to follow the solution by beginning in the reservoir (T=1) and tracing along the appropriate curve in Figure 2.5.2 until the narrowest section of the channel is reached. (Two of the reservoir states are drawn in the figure insets at the right.) If the narrowest section is reached before the dashed line is encountered, the solution is subcritical with no hydraulic transition. Downstream of the narrows, the solution is obtained by retracing the solution curve back towards T=1 as the channel widens. All such solutions are non-separated. If T at the narrows happens to be the critical T_c, then the dashed curve is crossed there and the downstream flow is supercritical. All supercritical branches of the solution curve terminate on the line $\bar{d}=1$ indicating flow separation for sufficiently large w. If the narrows is sufficiently constricted that $T<T_c$ for that curve, a complete steady solution cannot be constructed. In this case a time-dependent adjustment must occur, perhaps resulting in a change in q, ψ_i, or both. Figure 2.5.2 suggests that, in the absence of changes in ψ_i the upstream depth must *increase* to accommodate the narrower width.

A limiting case is q=2 corresponding to separation of the reservoir flow from the left wall. Here the outflow transport is the maximum that can be carried by the left boundary layer ($q^*=Q^*_{max}$). Higher transports are possible in general, but these require flow in the right boundary layer. When the flow in the reservoir is separated it is also critical, as suggest by the figure or by (2.2.26). Downstream of the reservoir, the channel would have to remain infinitely wide to sustain a solution.

Next consider the opposite case of variable topography with constant width. Since we have already assumed the reservoir to be infinitely wide, it is convenient to imagine the reservoir narrowing to a finite value, during which h remains zero, followed by a constant-width section containing a sill. Figure 2.5.2 is used to track the solution over the variable section of channel and Figure 2.5.3, which shows solution curves for variable h and fixed width (w^*/L_d=.75 or T=.63), is then used to continue further. The solution space of Figure 2.5.3 is divided into two regions: the upper portion ($\bar{d}>1$), for which the flow is non-separated and the dependent variable is $\bar{d}$, and the lower portion ($\bar{d}<1$), for which the flow is separated and T_e is the dependent variable. As before, ψ_i=1 and critical flow is marked by a dashed line.

If one begins at the upstream end of the uniform width section, where h=0 and where the flow is subcritical, the solution lies along the upper left hand border of Figure

2.5.3. Increases in h cause $\bar{d}$ to decrease as one follows the appropriate q^{-1}=constant curve. There are now two scenarios depending on the value of the interior reservoir depth. If q^{-1}<3.5 the flow will become critical *before* the separation point $\bar{d}$ =1 is reached, so that separation will occur downstream of the sill. This behavior occurs for relatively low sills (h_m<1.5). If $D_\infty / D > 3.5$ the flow separates upstream of the sill (while it is still subcritical) and remains subcritical until it reaches the sill, where it becomes critical. This situation, which is predicted when the interior reservoir surface elevation and the sill elevation are relatively high, has proven difficult to produce in laboratory or numerical experiments (e.g. Shen 1981 or Pratt *et al*. 2000).

(d) Transport relations.

The essential nature of upstream influence in a hydraulic model is expressed as a relationship between the parameters that characterized the basin flow and the control section geometry. In the nonrotating models discussed earlier, and in the WLK model, this relationship takes the form of a 'weir formula' in which the volume transport Q^* is written in terms of the basin surface elevation Δz^* above the sill. The situation in the Gill model is more complicated; for one thing the surface elevation varies across the upstream basin. The weir relationship is most easily expressed for the case of separated flow at the critical section. If (2.5.9) is applied there and (2.5.10) is used to eliminate T_{ec} from the resulting equation, one obtains

$$h_c = q^{-1} - 2 + (1 - \psi_i)q \ . \qquad (2.5.13)$$

Because of Gill's choice of the scaling factor $D=(fQ^*/2g)^{1/2}$, the volume flux is hidden in the nondimensionalization. The scaling relations

$$h_c = \frac{h_c^*}{(fQ^*/2g)^{1/2}}, \ q^{-1} = \left(\frac{2gD_\infty^2}{fQ^*}\right)^{1/2}, \text{ and } \ \psi_i = \frac{2\psi_i^*}{Q^*}$$

allow (2.5.13) to be recast as a formula for the transport:

$$\left(\frac{fQ^*}{2g}\right)^{1/2} = D_\infty - \left(D_\infty h_c^* + \frac{f\psi_i^*}{g}\right)^{1/2} \qquad (2.5.14)$$

(see Exercise 4.) In contrast to the nonrotating case and the zero potential vorticity case, two measurements in the reservoir are now needed to compute the volume flux Q^*. A depth measurement in the reservoir interior gives D_∞ while a depth measurement along either wall and use of the geostrophic relation gives ψ_i^*. Of course, depth measurements on both sidewalls would give the geostrophic transport directly and thus the utility of (2.5.14) is called into question. An alternative is discussed in the next chapter.

© L. Pratt and J. Whitehead 7/27/06
very rough draft-not for distribution

For non-separated flow the situation is more difficult. Applying (2.5.6) at the critical section, adding $\bar{d}_c$ times (2.5.5), and multiplying the result by $q/2$ gives

$$h_c = (1-\tfrac{1}{2}T_c^2)q^{-1} - \tfrac{3}{2}(1-T_c^2)\bar{d}_c - (\psi_i + T_c^2\bar{d}_c^2)q\,, \qquad (2.5.15)$$

or, in dimensional terms:

$$h_c^* = (1-\tfrac{1}{2}T_c^2)D_\infty + \tfrac{3}{2}(T_c^2-1)\bar{d}_c^* - D_\infty^{-1}(T_c^2\bar{d}_c^{*2} + \psi_i^* f/g) \qquad (2.5.16)$$

In addition, the dimensional version of (2.5.6) is

$$(1-T_c^2)D_\infty\bar{d}_c^* + T_c^2\bar{d}_c^{*2} = \frac{f^2Q^{*2}}{4g^2\bar{d}_c^{*2}T_c^2} \qquad (2.5.17)$$

If the algebraic complexity were not prohibitive, a 'weir' relation could be obtained by eliminating $\bar{d}_c^*$ between the last two equations. In general, the relationship between Q^*, D_∞ and ψ_i^* for a given h_c^* must be determined numerically. This subject is pursued further in Section 2.6, where different choices of scales ~~and~~ of the upstream parameters lead to more elegant formulations.

(e) Limiting Cases

Another way to gain intuition about the behavior of controlled solutions over the space of the parameters q and ψ_I is to consider the limiting cases of wide and narrow channels. We begin with a channel having a large, uniform width ($w \to \infty$, or $T \to 1$) and containing variable h. Many of the novel features of the full problem are captured in this setting. Critical flow must occur at the sill and we first examine the case in which the sill flow is separated. The nondimensional relationship between the sill height and the upstream variables is given by (2.5.13). In addition (2.5.11) requires that $q^{-1} \geq 2$ with marginal separation corresponding to $q^{-1}=2$. In this regime it is also possible for the upstream flow to be separated and the value of h_c at marginal separation can be calculated by evaluating (2.5.9) in the reservoir (h=0) and setting T_e=1. If (2.5.13) is then used to eliminate ψ_i from the resulting relation, one finds

$$h_c = \frac{3+(1-q^{-1})^2}{2q^{-1}} - 1 \qquad (2.5.18)$$

The case of attached flow is more subtle. In Section 2.2 we showed that the characteristic speed of a left-wall Kelvin wave for T=1 is proportional to the negative of the depth at the left wall (see 2.2.26). The flow must therefore be subcritical if it is

attached at the left wall, a finding that rules out critical control of attached flow in the problem under consideration. If however, the channel width is considered to be large but finite, a class of attached, critically controlled flows arises. These solutions are described by expanding (2.5.6) and (2.5.15) in powers of $1-T_c^2$. The former becomes

$$\bar{d}_c = 1 + \tfrac{1}{4}(1-T_c^2)(2-q^{-1}) + O[(1-T_c^2)^2], \qquad (2.5.19)$$

showing that marginal separation ($\bar{d}_c \to 1$) occurs as $1-T_c^2 \to 0$ as anticipated. However, the first correction to this limit allows the possibility of attached flows $\bar{d}_c > 1$ provided that $q^{-1}<2$. These flows are close to separation at the critical section and the relationship between the upstream variables and h_c is obtained by substituting (2.5.19) into (2.5.15) and expanding the results. The end product is

$$h_c = \tfrac{1}{2}q^{-1} - q(1+\psi_i) + O(1-T_c^2). \qquad (2.5.20)$$

Equations (2.5.13) and (2.5.20) relate the sill height to the upstream conditions for a hydraulically controlled flow for the cases of separated and non-separated flow at the control section. The dimensional versions of these relations could be recast as transport (or 'weir') formulas. Figure 2.5.4 shows the solutions to the two relations, with ψ_i plotted as a function of h_c and q^{-1}. Each point in the diagram represents a specific, hydraulically controlled flow. In the upper part of the figure ($q^{-1}>2$) the flow is separated at the critical section, here the sill. Since the effective width w_{ec} of the separated flow is determined completely by q^{-1}, these widths have been indicated along the right-hand border of the figure. The dashed curve is determined by (2.5.18) and the region lying to left corresponds to flows that are also separated in the upstream basin, so that no contact with the left wall is made along the entire length of channel. All such solutions have $\psi_i>1$, implying that the approach flow in the reservoir is along the left-hand free edge and that some of this flow returns upstream along the right wall before reaching the sill, as shown in Inset A. Such a solution could be considered a coastal flow forced by along-shore changes in topography. To the immediate right of the dashed region the upstream flow is non-separated but the flow at the sill is separated. In addition the approach flow is concentrated in the left-hand boundary layer, as sketched in Inset B. Continuing to move to the right into regions of higher sill elevation, one enters a region where $-1 \le \psi_i \le 1$, so that the approach flow is unidirectional, as shown in Inset C. One of the interesting aspects of cases A, B, and C is that the critical width w_{ec} is often O(1) or less. Thus, approach flow along the left-hand edge can cross the channel and be carried close to the right hand boundary at the sill. The remaining region in the upper part of the figure ($\psi_i<-1$) corresponds to approach flow along the right hand wall with some return flow along the left-hand wall, as sketched in Inset D.

In the lower part ($q^{-1}<2$) of the figure, the flow is marginally attached at the sill. Since $\psi_i \le 1$ in this lower region, the upstream flows are either unidirectional or approach along the right-hand wall and partially return along the left-hand wall, as sketched in Insets E and F. One of the interesting characteristics of the type F flows is that the

surface or interface elevation in the interior of the reservoir can be lower than the sill elevation ($D_\infty < h_c$). [This can be shown by holding $q^{-1}(= D_\infty / D)$ constant in (2.5.19) and taking ψ_i sufficiently negative and large.] Only the interior interface elevation is below the sill; the elevation along the right-hand wall remains above it.

It is also natural to inquire after the dynamics that allow the upstream flow to cross from the right to the left side of the channel before the sill is reached. What happens, in fact, is that a weak along-channel pressure gradient exists in the interior, supporting a cross-channel geostrophic flow. Since $d = q^{-1}$ and $v \cong 0$ in the channel interior, the *y*-momentum equation reduces to

$$u \cong -\frac{\partial h}{\partial y}.$$

On the upstream face of the obstacle $\partial h / \partial y > 0$, a negative (right-to-left) geostrophic flow exists, whereas the opposite situation occurs on the downstream face.

The Gill model is rather difficult to digest and it is worth recapping some of the highlights. These include the introduction of the concept of *potential depth* D_∞ and the appearance of a global deformation radius $L_d=(gD_\infty)^{1/2}/f$, which is uniform throughout the fluid regardless of the local depth. Another novel feature is the containment of the flow in boundary layers of width L_d. Exploitation of this structure in the wide upstream reservoir allows one to use ψ_i as a parameter in place of the less intuitive $\overline{B}$. Critical control of the flow is exercised by Kelvin waves or their frontal counterparts, both of which are trapped to side walls or free edges. Another new feature of Gill's model is that three dimensional parameters ($Q^*, D_\infty,$ and ψ_i^*) are needed to specify the upstream state. If the flow is hydraulically controlled, so that Q^* is a function of D_∞ and ψ_i^*, then just the latter two are needed. Thus, a 'weir' formula relating Q^* to a single upstream depth is not possible without further approximation. Finally, some of Gill's solutions exhibit interesting new behavior including counterflows, crossing of the fluid from one side of the channel to the other over great distances, and instances in which the interior reservoir interface level lies below the sill level

f. Experiments.

As described in the Section 2.4, Shen (1981) set up a series of experiments designed to produce steady, rotating channel flow with uniform potential vorticity. The upstream basin has a horizontal bottom or adjustable depth, allowing the nominal value of the potential vorticity to be varied. Cases of hydraulically controlled flow and submerged weir flow were reproduced and compared to theories. The fundamentals of the submerged weir theory were described in the previous section and the resulting formulas for volume flux are listed by Shen only for the case of zero potential vorticity. For controlled flow, the flux prediction is based on a version of the Gill (1977) that employs a different scaling and that assumes that all flow enters the channel along the left

wall (ψ_i=1). The volume flux can then be scaled in such a way as to depend only on the single parameter $w^*f/(gD_\infty)^{1/2}$. We have already shown that this parameter is a measure of the potential vorticity, the 'zero potential vorticity' limit corresponding to vanishingly small values. As shown in Figure 2.5.5, agreement between experiment and theory is good and is best for small or moderate values of $w^*f/(gD_\infty)^{1/2}$. Shen suggests that the disagreement of about 10% for moderate values is due to the effects of non-uniform upwelling in the upstream reservoir, producing non-uniform potential vorticity.

Exercises

1) Show that setting $D = (fQ^*/2g)^{1/2}$ is equivalent to setting Q =2.

2) In connection with (2.5.8) show that $[T_c^{\,4}(\bar{d}_c - q^{-1})^2 - \bar{d}_c^{-2}] = 0$ implies that $v_c(w/2, y) = d_c(-w/2, y) = 0$.

3) By following the steps outlined below, show that non-separated flow at a critical section must be unidirectional in $-w/2<y<w/2$ provided that the (uniform) potential vorticity is non-negative. Further show that separated critical flow must have $v(w/2,y)=0$.

(a) Use the result of Problem 1 of Section 2.2 to argue that the flow is unidirectional at any y provided that $v(y,w/2)$ and $v(y,-w/2)$ do not differ in sign.

(b) Introduce the quantity $r = \hat{v}/\bar{v}$ and argue that the flow is unidirectional for $|r| < 1$ and has $v(y,w/2)=0$ for r=-1. Further show that $r = T^2\bar{d}(\bar{d} - q^{-1})$

(c) Using the critical condition (2.5.6) along with (2.5.1), show that

$$r = \frac{T_c^2\bar{d}_c^2 - \bar{d}_c^{-2}}{1 - T_c^2}$$

and deduce that r=-1 when the flow is separated from the left wall($\bar{d}_c$=1).

(d) For attached flow ($\bar{d}_c$>1) show that r>-1. Then show that the requirement of non-negative potential vorticity and the result of (c) lead to $r \le 1$.

4. Obtain the transport relation

$$\left(\frac{fQ^*}{2g}\right)^{1/2} = D_\infty \pm \left(D_\infty h_c^* + \frac{f\psi_i^*}{g}\right)^{1/2}$$

by writing (2.5.13) in dimensional units. Next, show that only the '-' sign is appropriate. (Hint: one way to do this is to consider the case of an infinitely wide channel and with no flux in the right-wall boundary layer.)

5. *The limit of small potential vorticity:* ($q<<1$).
Since $q = \left(fQ^*/2gD_\infty^2 \right)^{1/2}$ this limit can be achieved by fixing Q^* and increasing D_∞.

(a) Show that the critical condition for attached flow (2.5.6) requires that

$$\bar{d}_c = \left(\tfrac{1}{2} w_c\right)^{-2/3} + O(q).$$

(b) Using (2.5.15) and the above result, show that

$$h_c = q^{-1} - \tfrac{1}{2}(\tfrac{1}{2} w_c)^2 - \tfrac{3}{2}(\tfrac{1}{2} w_c)^{-2/3} + O(q).$$

provided ψ_i remains fixed. Thus the sill height must (to lowest order) increase in proportion to the interior reservoir depth q^{-1} (dimensionally D_∞).

(c) Show that dimensionalization of the result in (b) leads to the WLK transport formula (2.4.10) for attached flow.

Figure Captions

2.5.1 Gill's (1977) ideal of the upstream basin or reservoir.

2.5.2 Solution curves for flow through a pure contraction. Note that $T = \tanh(q^{1/2} w/2)$.

2.5.3 Solution curves for flow over a sill in a constant width channel. The lower half of the diagram applies to separated flow, with $T_e = \tanh(q^{1/2} w_e/2)$.

2.5.4 Regime diagram showing various states of separation and recirculation for flow in an infinitely wide channel with a sill. Solutions to the left of the dashed line are entirely separated from the left wall. Those lying below the line $q^{-1}=2$ are attached at and upstream of the sill.

2.5.5. The curve gives the predicted volume flux Q' as a function of $w^*f/(gD_\infty)^{1/2}$ for critically-controlled flows observed in the Shen (1981) experiment. The crosses give the experimental values. The transport has been scaled by its value at $w^*f/(gD_\infty)^{1/2}=0.3$, corresponding to the deepest upstream depth D_∞ used in the range of experiments.

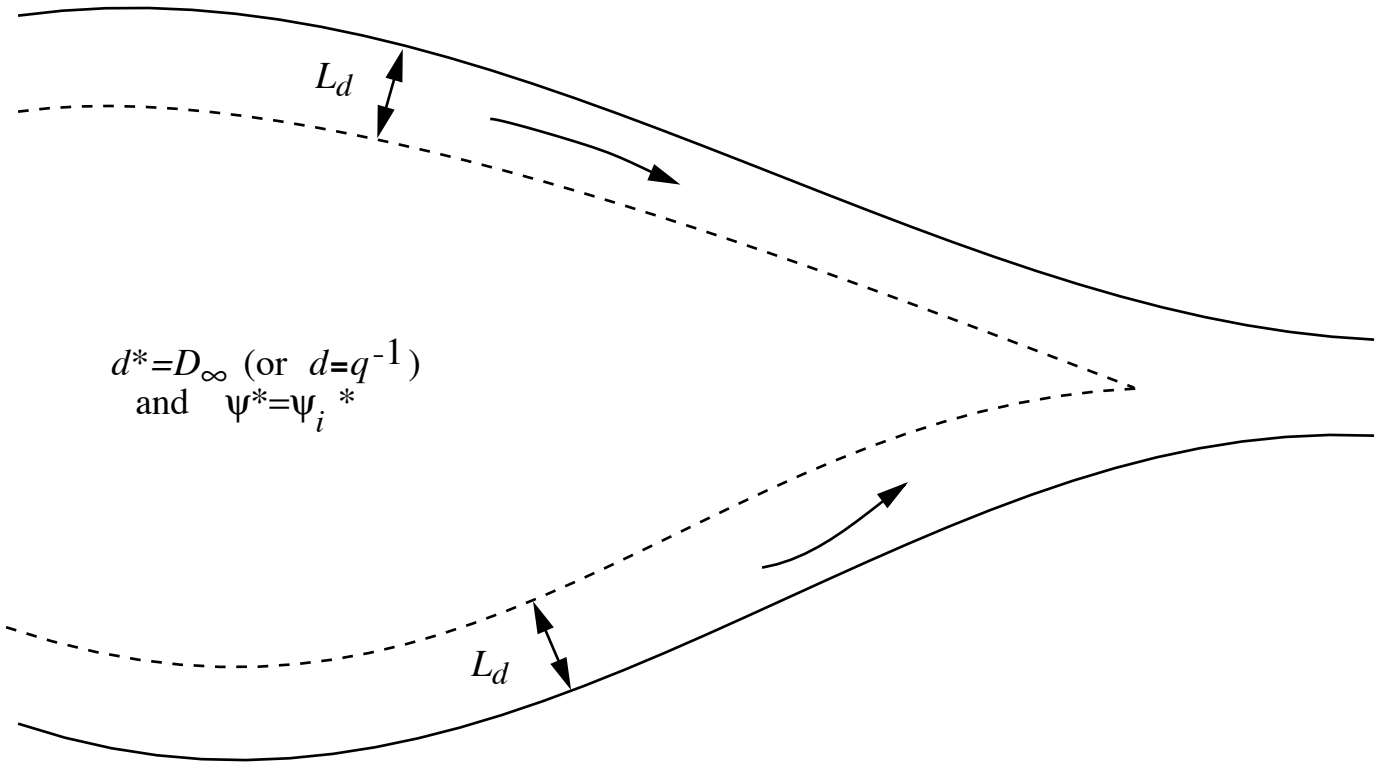

Figure 2.5.1

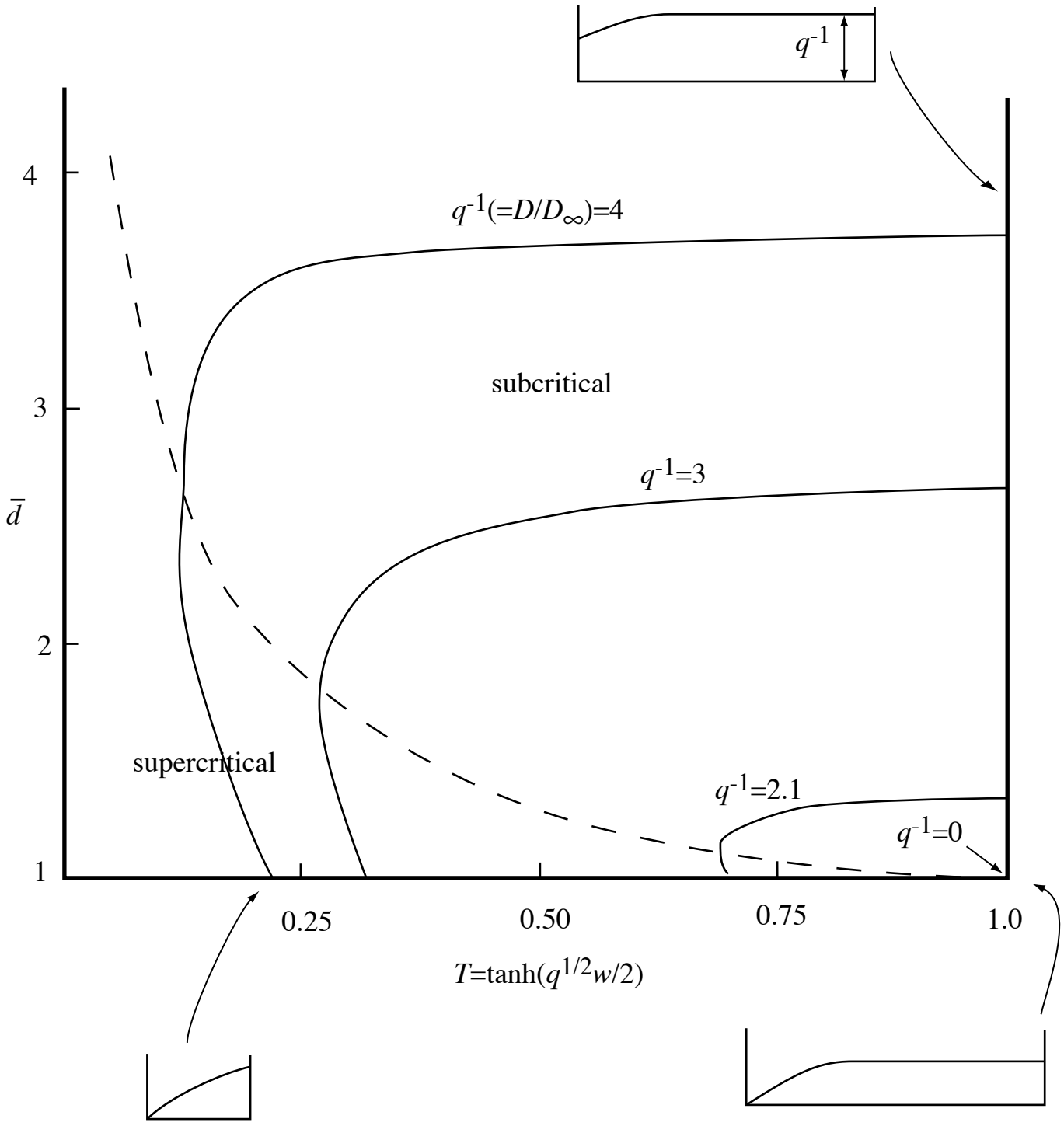
q^{-1}
4
3
2
1
$\bar{d}$
$q^{-1}(=D/D_\infty)=4$
subcritical
$q^{-1}=3$
supercritical
$q^{-1}=2.1$
$q^{-1}=0$
0.25
0.50
0.75
1.0
$T=\tanh(q^{1/2}w/2)$

Figure 2.5.2

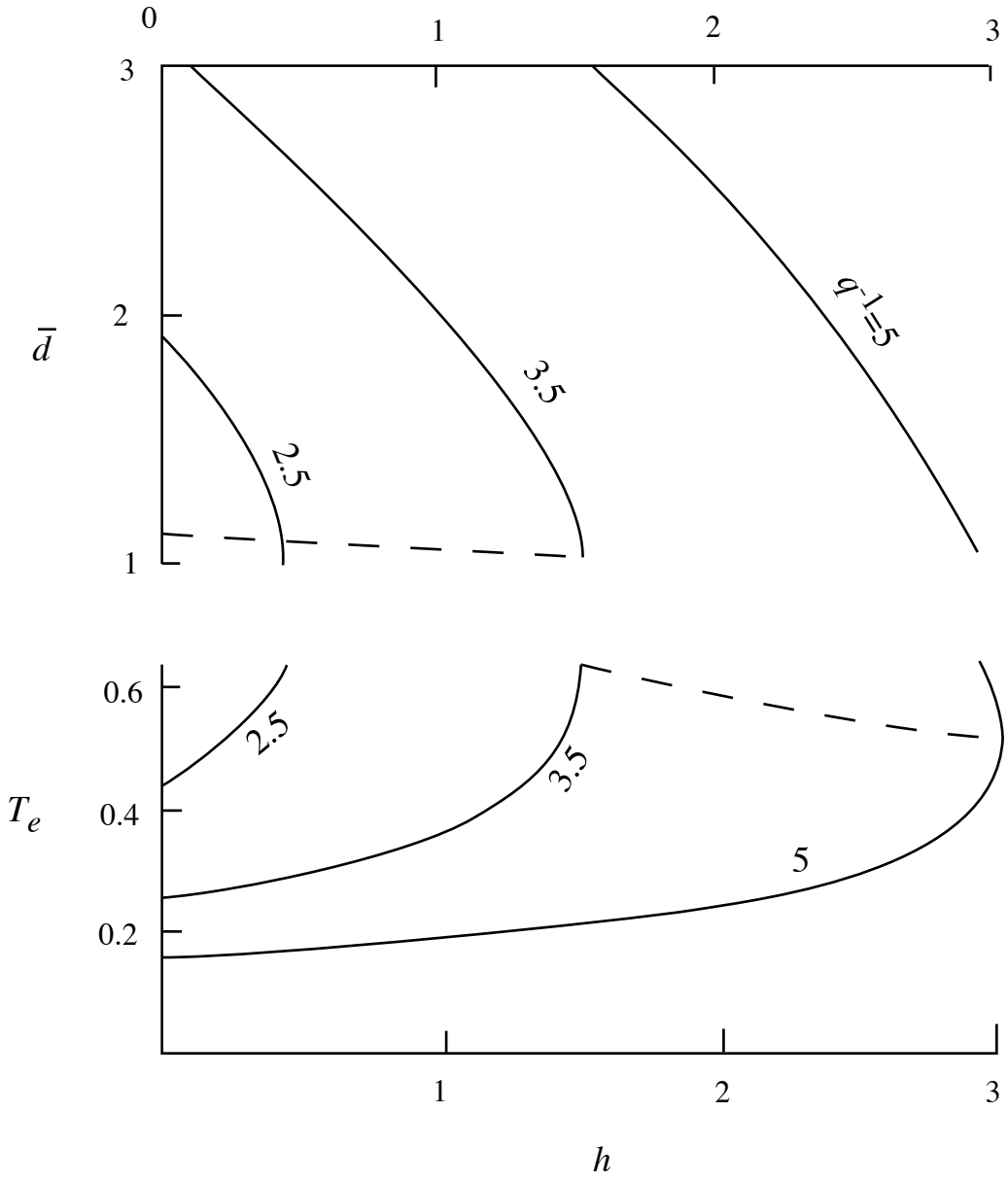

Figure 2.5.3

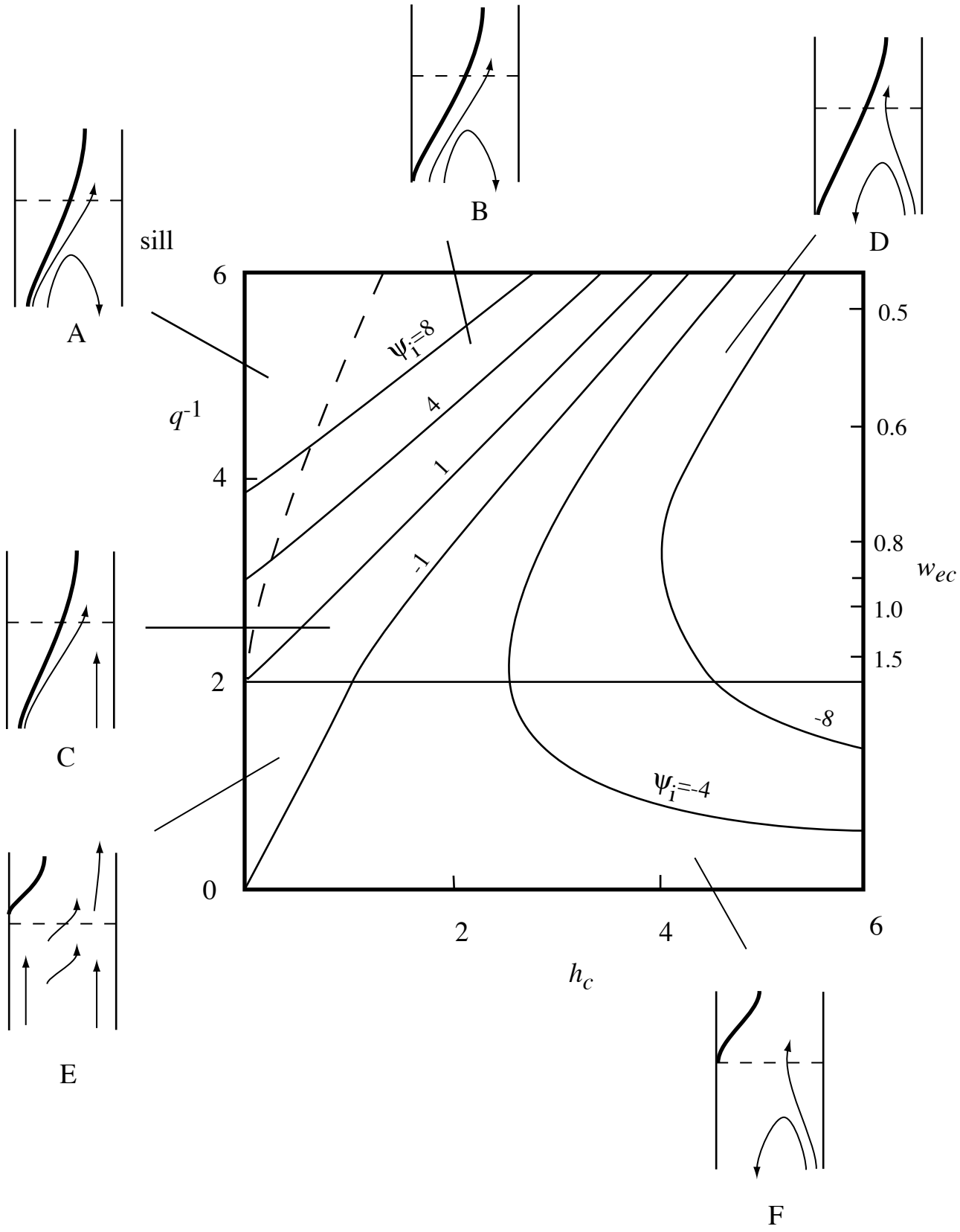

Figure 2.5.4

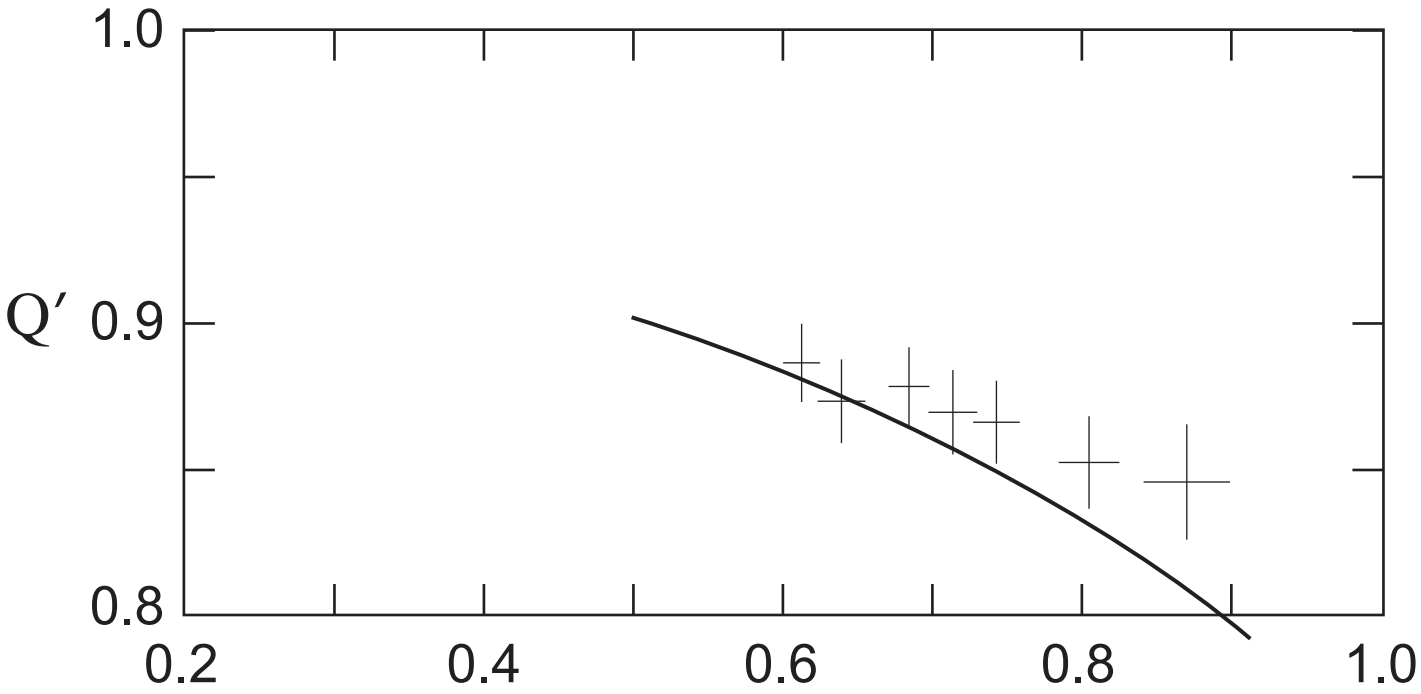

Figure 2.5.5